ELSEVIER

Journal of Alloys and Compounds 230 (1995) 67–75

Journal of ALLOYS AND COMPOUNDS

Precipitation phenomenon in stoichiometric $Nd_2Fe_{14}B$ alloys modified with titanium and titanium with carbon

D.J. Branagan, R.W. McCallum

Ames Laboratory, USDOE and Department of Material Science and Engineering, Iowa State University, Ames, IA 50011, USA

Received 29 March 1995; in final form 13 April 1995

Abstract

Precipitation phenomenon has been investigated in stoichiometric $Nd_2Fe_{14}B$ alloys modified with Ti and Ti with C. Precipitates can be used to inhibit grain growth and understanding the precipitation process is important in order to form the most effective dispersion. In the Nd–Fe–B–Ti system, TiB_2, and in the Nd–Fe–B–Ti–C system, TiC are found to be the precipitating phases. Depending on composition, the precipitates can form at high temperatures in the liquid, during cooling after solidification, and during heat treatment. The precipitates form on grain or phase boundaries. The TiC precipitates typically form as discrete particles while the TiB_2 precipitates form generally in a globular bunched-up fashion. After a homogenization heat treatment, the equilibrium solubilities of Ti and Ti with C in the $Nd_2Fe_{14}B$ phase are found to be 0.47 wt.% and ≤0.06 wt.% respectively. This means that almost all of the alloyed Ti and C can be precipitated as TiC which returns the excellent intrinsic magnetic properties of the hard magnetic phase. Both the carbides and the borides are found to have excellent high-temperature stability and resist coarsening and dissolution at least to 1000°C. Since Ti and C react to form TiC the amount of hard magnetic phase is not reduced while Ti addition alone reacts with boron and reduces the amount of hard magnetic phase if extra boron is not added.

Keywords: Titanium; Carbon; Precipitation phenomena; $Nd_2Fe_{14}B$ alloys

1. Introduction

Precipitation in the 2–14–1 system is important for both rapid solidification processing and in the powder route for making permanent magnets, since the coercivity is intimately tied to the grain size of the hard magnetic phase in materials made from both methods of permanent magnet production [1–3]. In order to achieve a uniform fine grain size which is stable during thermal processing, a uniform dispersion of a stable second phase may be used. A physical metallurgical study was launched to look at the effects of Ti and Ti with C addition to the $Nd_2Fe_{14}B$ (2–14–1) system. The formation, solubility, and stability of the precipitating phases will be studied. Precipitates form at surfaces in the microstructure including phase boundaries, grain boundaries, dislocations, etc., because surfaces provide sites for heterogeneous nucleation. In order to form secondary phases, the precipitating elements must come out of liquid or solid solution. Therefore the solubilities of the alloying elements must be known in order for precipitation to be understood. This includes an understanding of the liquid and solid solubility as well as the equilibrium and non-equilibrium solubility. The maximum precipitate pinning force at the grain boundaries increases as the volume fraction of the precipitates increases and as the size decreases [4]. In order for the precipitates to effectively prevent grain growth, they must form an effective dispersion and be stable at high temperatures. Both dissolution and coarsening (Ostwald ripening) will diminish the effective pinning force.

Since the $Nd_2Fe_{14}B$ phase is a ternary phase, alloying is complicated by the reactivity of the individual elements. The ideal alloying addition would not react with the constituent elements of the phase since that would reduce the amount of the hard magnetic phase. However, if a reaction occurs the starting composition may be adjusted in some cases to compensate for the loss of the particular element. In Table 1, the stable phases from binary phase equilibria are shown which might form from the addition of Ti and C to Nd–Fe–B.

SSDI 0925-8388(95)01700-3

Table 1
Stability binary phases

System	Phases	Enthalpies (KJ (g at)$^{-1}$)	Ref.
Nd–Ti	None		
Fe–Ti	TiFe		
	$TiFe_2$		
B–Ti	TiB		
	Ti_3B_4		
	TiB_2	−108.0	11
Nd–C	NdC_2	−29.6	9
	Nd_2C_3	−20.45	9
Fe–C	Fe_3C	6.3	11
B–C	B_4C	−12.535	10
TiC	Ti_2C		
	TiC	−92.1	11

This table is only partially complete since it does not list ternary or higher-order phases or metastable phases that can be stabilized by impurity elements or the surrounding lattice. From Table 1, it can be seen that the TiB_2 and the TiC phases are by far the most stable phases listed. When Ti is added to the 2–14–1 system it might be expected that TiB_2 will form owing to its extremely high free energy of formation. When Ti and C are added to the 2–14–1 system, the binary-phase free energies indicate that TiB_2 would form preferentially to TiC. However, the balance of free energies leading to equilibrium in a multicomponent system does not necessarily agree with the binary phase equilibrium.

In this paper, the study of ingots gives an understanding of the alloy chemistry and phase equilibrium involved in the precipitation process. In addition, the study of as-cast and homogenized ingots will be used to gain an understanding of the solubilities of the additive elements and the stabilities of the precipitating phases. The results from this paper will be useful in the powder route to making permanent magnets and can be related to the precipitation processes occurring on a much finer scale in rapidly solidified samples.

2. Experimental procedure

All alloys used were made by arc-melting the elements on a water-cooled copper hearth. The compositions of the alloys studied are found in Table 2. Compositions are given in the form $(Nd_{2/17}Fe_{14/17}B_{1/17})_{100-X}$ + Addition$_X$. The purity of the starting elements used were 99.95 wt.% Nd, 99.99 wt.% Fe, 99.5 wt.% B, 99.97 wt.% Ti, and spectrographic grade C. The arc-melted ingots were melted and flipped several times, broken up, and arc-melted again to insure homogeneity. 10 g samples were studied to minimize macrosegregation. The average weight loss after arc-melting was less than 0.02 wt.%. Heat treating was performed by wrapping the arc-melted ingots in tantalum foil and then sealing them in a quartz tube under 0.5 atm argon. The homogenization heat treatment was carried out at 1000°C for one week in a box furnace. Cross-sections of the as-cast and homogenized ingots were mounted with diallyl phthalate. The samples were polished using standard metallographic techniques without etching. Microstructural studies were performed with a Jeol JSM 6100 scanning electron microscope (SEM). Energy dispersive spectroscopy (EDS) was performed with an Oxford Link Pentaset Detector. Semiquantitative analysis was achieved using a Ti standard with the appropriate *ZAF* (atomic number, absorption, fluorescence) corrections on MICROPLUS software made by Dapple. The wt.% Ti dissolved in the α-Fe and 2–14–1 phases is reported as an average of at least five independent measurements. X-ray diffraction scans were carried out on powdered samples with Cu Kα radiation from a Phillips X-ray diffractometer.

3. Results and discussion

3.1. As-cast ingots

3.1.1. Nd–Fe–B–Ti system

The as-cast $X = 2$ Ti and $X = 6$ Ti alloys can be seen in Figs. 1 and 2 respectively. The usual ternary

Table 2
Composition of alloys studied

Alloy	Composition	X Ti added	X C added
Base	$Nd_{2/17}Fe_{14/17}B_{1/17}$		
$X = 2$ Ti	$(Nd_{2/17}Fe_{14/17}B_{1/17})_{100-x} + Ti_x$	2	
$X = 6$ Ti	$(Nd_{2/17}Fe_{14/17}B_{1/17})_{100-x} + Ti_x$	6	
$X = 2$ C	$(Nd_{2/17}Fe_{14/17}B_{1/17})_{100-x} + C_x$		2
$X = 6$ C	$(Nd_{2/17}Fe_{14/17}B_{1/17})_{100-x} + C_x$		6
$X = 2$ TiC	$(Nd_{2/17}Fe_{14/17}B_{1/17})_{100-2x} + Ti_xC_x$	2	2
$X = 6$ TiC	$(Nd_{2/17}Fe_{14/17}B_{1/17})_{100-2x} + Ti_xC_x$	6	6

Fig. 1. SEM image of an as-cast $X = 2$ Ti alloy. Arrows indicate the location of the TiB_2 precipitates.

solidification sequence was found with properitectic, peritectic, and eutectic phases formed [5]. The microstructures of the two alloys were similar except rod-shaped precipitates approximately 3–12 μm long and 1–3 μm in diameter were found in the $X = 6$ Ti alloy (labeled 1 in Fig. 2). From EDS semiquantitative analysis, the primary rod-shaped precipitates on average consisted of 56.1 wt.% Ti. No other characteristic radiation was detected so the balance is presumably boron whose characteristic energy is sufficiently low to be absorbed by the thin window of the EDS detector. The amount of Ti measured is a little lower than the expected value of 68.8 wt.% Ti in the TiB_2 phase. However, due to the spot size of the electron beam some of the surrounding matrix phase was probability measured which would contribute to a lower value for

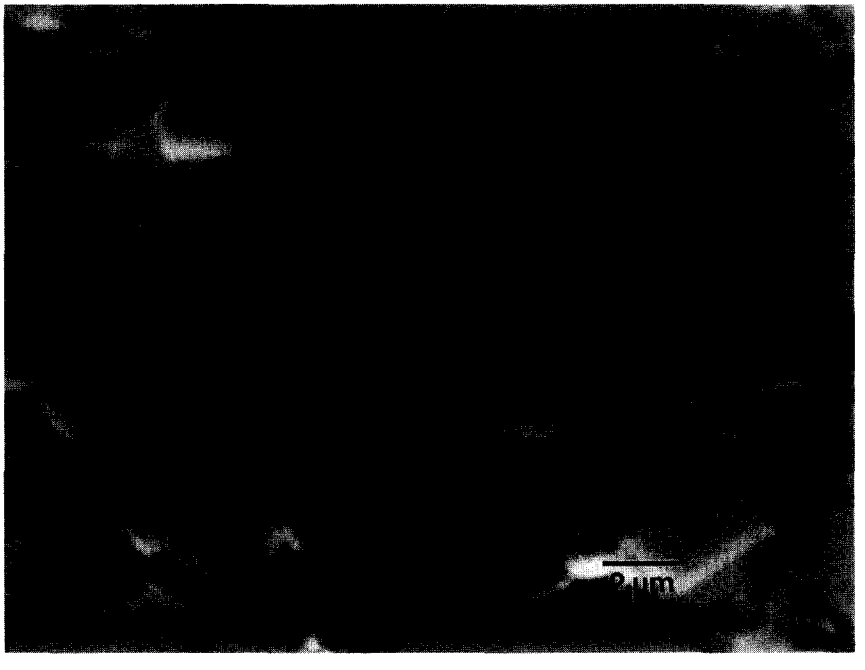

Fig. 2. SEM image of an as-cast $X = 6$ Ti alloy. Primary and secondary TiB_2 precipitates are laelled 1 and 2, respecti

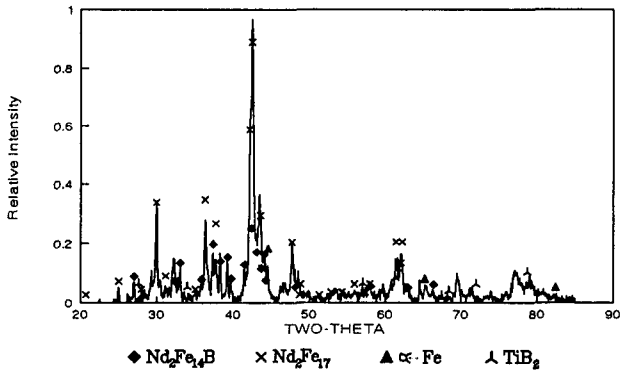

Fig. 3. XRD pattern of an as-cast Ti alloy.

this measurement. The TiB_2 phase has been found in the 2–14–1 system elsewhere [6,7] and X-ray diffraction scans verified that the Ti-rich precipitates are the TiB_2 phase. The X-ray diffraction scan of the as-cast $X = 6$ Ti alloy can be seen in Fig. 3. Along with the TiB_2 phase, α-iron, Nd_2Fe_{17}, and $Nd_2Fe_{14}B$ phases were found. Note that the shape, size, and distribution of the TiB_2 precipitates indicated that the precipitates formed in the liquid since the liquid solubility of the $X = 6$ Ti alloy had been exceeded.

Table 3
Wt.(%) Ti dissolved

Alloy X	As-cast		Homogenized	
	2–14–1	α-Fe	2–14–1	2–17
2 Ti	1.1	1.3	0.5	
6 ti				2.2
2 TiC	1.3	1.7	0.06	
6 TiC	1.2	1.7	0.02	

In the as-cast microstructures additional small titanium-rich precipitates with an acicular morphology were found ranging in size from 0.5 to 1 μm long. These precipitates formed at the grain boundaries of the matrix phase in a typically continuous manner. These secondary precipitates formed during cooling and after solidification and are probably the TiB_2 phase. Not many precipitates were found because the precipitation process upon solidification exhibits C-curve kinetics. That is, there is a peak precipitation temperature where the diffusion rate and driving force is maximized. There is simply not enough time during the peak-temperature range for the precipitation process to occur to any significant extent due to the fast cooling rate occurring on a water-cooled copper hearth.

The presence of the secondary boride precipitates indicate that titanium is being trapped during solidification in supersaturated solid solution. The measured solubilities of Ti in the α-Fe and 2–14–1 phases can be seen in Table 3. In this $X = 6$ Ti alloy, the wt.% Ti dissolved in the as-cast phases was not determined due to the difficulty in distinguishing between the 2–17 and 2–14–1 phases. These results show that Ti has significant solubility in both the iron and 2–14–1 phases. Note that no titanium was found in the rare earth-rich eutectic phases.

3.1.2. Nd–Fe–B–Ti–C system

In Figs. 4 and 5, the as-cast $X = 2$ TiC and $X = 6$

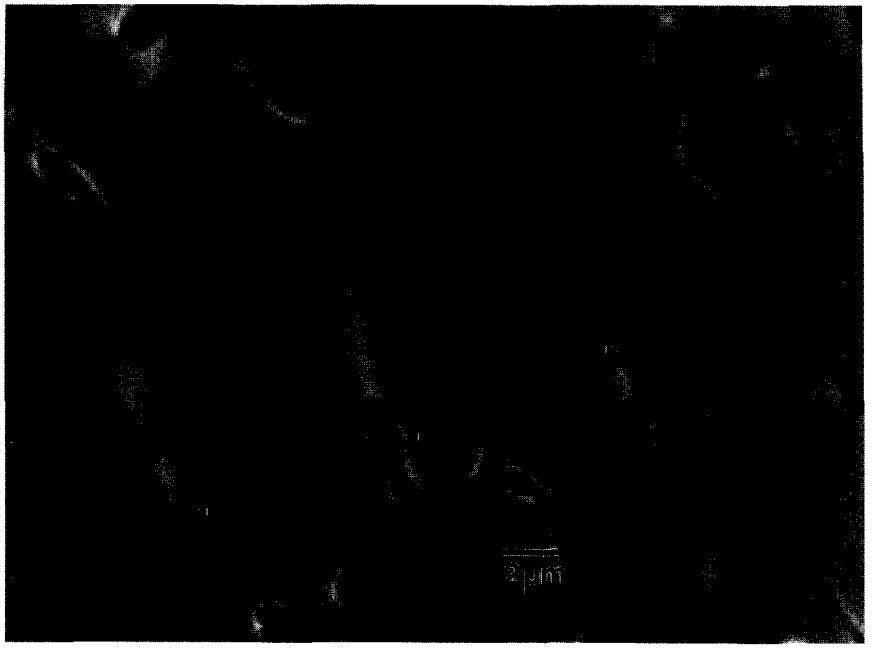

Fig. 4. SEM image of an as-cast $X = 2$ Ti alloy. Arrows indicate the location of the TiC precipitates.

TiC alloys can be seen respectively. The usual ternary solidification sequence was found for both alloys, however in the $X = 6$ TiC alloy, Ti-rich precipitates from 10 to 20 μm long with a cubic morphology formed (labeled 1 in Fig. 5). From EDS, the primary carbides are found to be 80.7 wt.% Ti which is very close to the expected value of 80.0 wt.% Ti in the TiC phase. Carbon intensity was also measured although it appeared that the signal was partially absorbed by the detector thin window. X-ray diffraction scans verified the formation of the TiC phase (Fig. 6). The primary precipitates appeared to have first formed from the liquid with a cubic shape and then partially reacted during solidification. Some of the primary carbides remained essentially cubic in form while others experienced a much greater degree of dissolution. The envisioned solidification scenario is as follows. First, at high temperature in the liquid, primary TiC cubic precipitates formed reaching an equilibrium of Ti and C in the liquid phase. Second, during solidification, properitectic iron dendrites formed which contained some Ti. To maintain the depleted liquid equilibrium some parts of the primary Ti-carbide precipitates redissolved.

The results show that in the quintery Fe–Nd–Ti–B–C system, TiC is found to be the most stable secondary phase. Apparently in the boron case, there is a free-energy balance between using the boron to form a TiB_2 or using the boron to form the 2–14–1 phase. The low stability of the $Nd_2Fe_{14}C$ phase alters the phase equilibrium and makes it more favorable in energy for TiC to form.

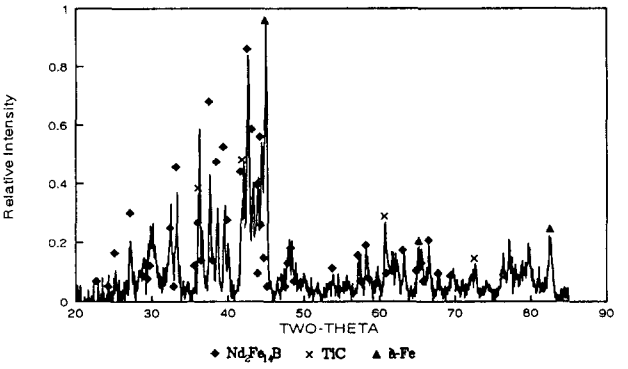

Fig. 6. XRD pattern for the as-cast $X = 6$ TiC modified alloy.

In the as-cast microstructures, secondary precipitation occurs as well with acicular-shaped Ti-rich precipitates present in the order of 0.5–1.0 μm long. Owing to the small size of the precipitates, semiquantitative analysis could not be performed on them but the phase equilibrium suggests that TiC is formed. The existence of the secondary precipitates indicate that titanium and carbon have been essentially trapped in supersaturated solid solution during solidification.

The solubilities of Ti in the as-cast phases can be seen in Table 3. Ti has at least a 1.3 wt.% non-equilibrium solubility in the 2–14–1 phase. It should be noted the value of the solubility observed in a phase upon solidification is very cooling-rate-dependent and since secondary carbide precipitation has occurred the maximum non-equilibrium solubility would be higher.

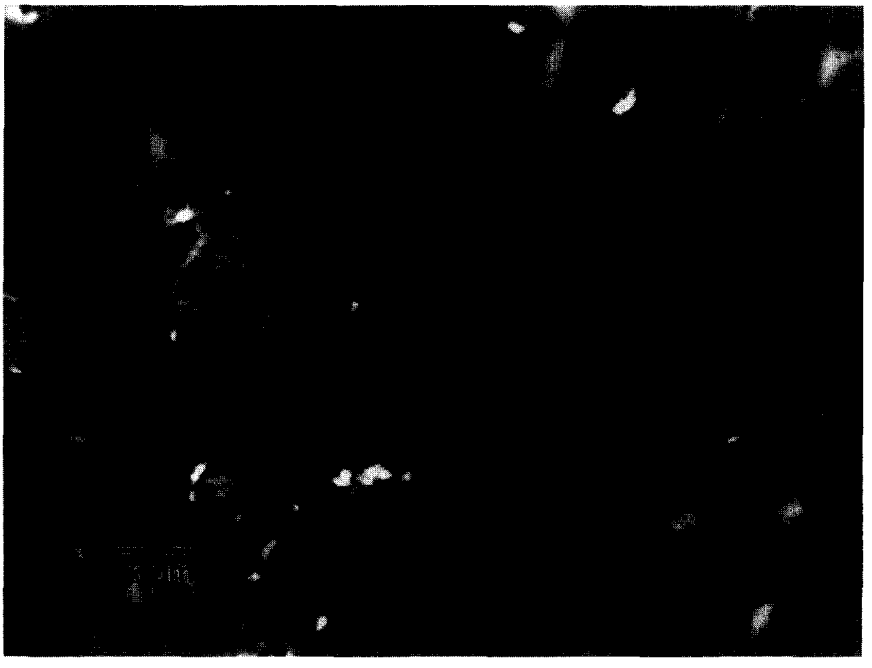

Fig. 5. SEM image of an as-cast $X = 6$ Ti alloy. Primary and secondary TiC precipitates are laelled 1 and 2, respectively.

3.2. Homogenized ingots

3.2.1. Nd–Fe–B–Ti system

During homogenization free iron reacts with the rare-earth eutectic phase to form more 2–14–1 phase. In the $X = 2$ and $X = 6$ Ti alloys secondary carbide precipitation occurred with many additional fine precipitates in the order of 0.5–1 μm long formed in the microstructures of both Ti-containing alloys (Figs. 7 and 8). These secondary precipitates are very similar in size and appearance to those formed initially during cooling after solidification. These precipitates formed

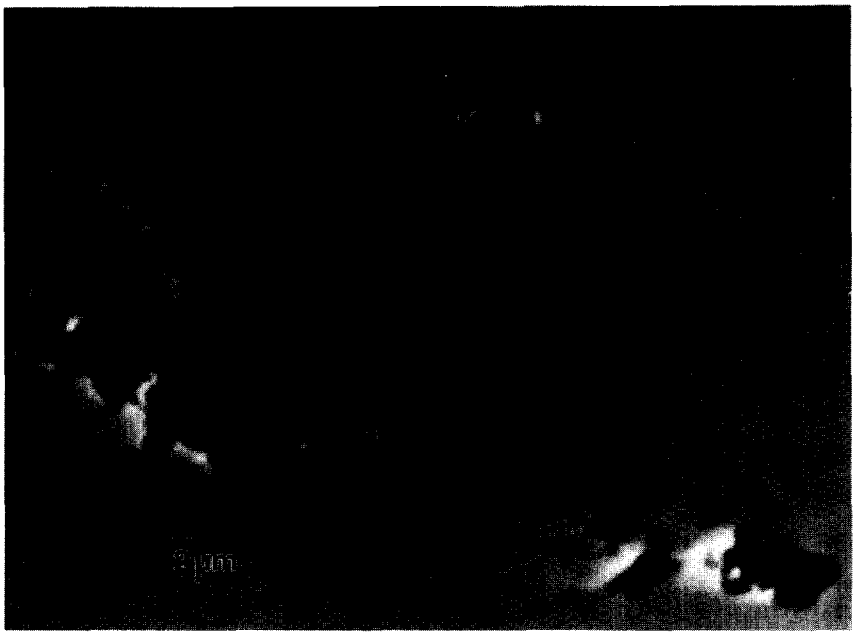

Fig. 7. SEM image of an $X = 2$ Ti alloy homogenized at 1000°C for one week. Arrows indicate colonies of TiB_2 formation.

Fig. 8. SEM image of an $X = 6$ Ti alloy homogenized at 1000°C for one week. Primary and secondary TiB_2 precipitates are labelled 1 and 2, respectively.

along the grain boundaries of the matrix phase in a bunched-up fashion typically as colonies (marked with arrows in Fig. 7).

After homogenization, the X-ray diffraction scan of the $X = 6$ Ti alloy indicates only the presence of TiB_2 and Nd_2Fe_{17} phases (Fig. 9). From stoichiometric considerations, there is more than enough Ti present in the alloy to react with all of the boron to form the TiB_2 phase with 2.8 wt.% Ti left over. Apparently this reaction occurred to completion which caused the remaining neodymium and iron to form the 2–17 phase. In the $X = 2$ Ti alloy, the Ti addition is less and the 2–14–1 phase is the main phase although the 2–17 phase exists as well.

The equilibrium solubility of titanium was measured

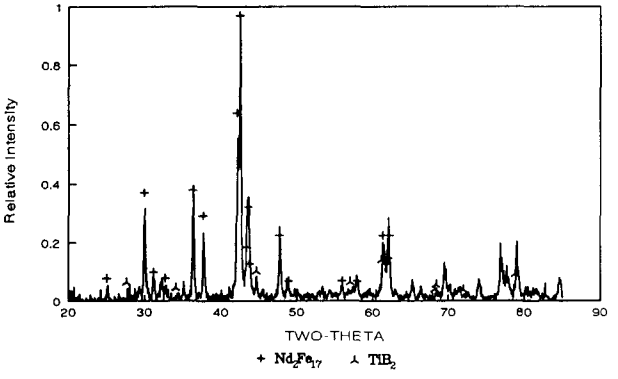

Fig. 9. XRD pattern for the $X = 6$ Ti modified alloy heat treated at 1000°C for one week.

for the 2–14–1 and 2–17 phases after homogenization (Table 3). In the $X = 2$ Ti alloy, it was found that 0.5 wt.% Ti remained in the 2–14–1 phase and in the $X = 6$ Ti alloy 2.2 wt.% Ti remained dissolved in the 2–17 phase. However it is surmised that if greater amounts of boron would have been present the equilibrium solubility would have been much lower due to the formation of TiB_2.

3.2.2. Nd–Fe–B–Ti–C system

During the homogenization heat treatment, secondary Ti-rich precipitates formed in both the $X = 2$ and $X = 6$ TiC alloys (Figs. 10 and 11 respectively). The X-ray diffraction scan indicates that a composite microstructure is formed consisting of only two phases; 2–14–1 and TiC (Fig. 12). The carbides were distributed in discrete 0.5–1 μm long particles along the matrix grain boundaries and also along the prior iron boundaries which had since homogenized (labeled 1 in Fig. 10). A TiC precipitate which formed at the triple junction between grains is labeled 3 in Fig. 11. The carbides which formed during cooling after solidification and those formed during homogenization are both similar in size and appearance. This might be expected since in both cases the precipitates formed from supersaturated solid solution.

After the homogenization heat treatment, only 0.06 wt.% and 0.02 wt.% Ti remained in the 2–14–1 phases of the $X = 2$ TiC and $X = 6$ TiC alloys respectively (Table 3). The equilibrium solubility may be even less than the measurements indicate owing to the many

Fig. 10. SEM image of an $X = 2$ Ti alloy homogenized at 1000°C for one week. Arrows indicate the location of the TiC precipitates. The TiC precipitates that formed on the dendritic iron boundaries which have since homogenized are labeled 1.

Fig. 11. SEM image of an $X = 6$ TiC alloy homogenized at 1000°C for one week. Primary and secondary TiC precipitates are labeled 1 and 2, respectively. A TiC precipitate that formed at the triple junction of the grains is labeled 3.

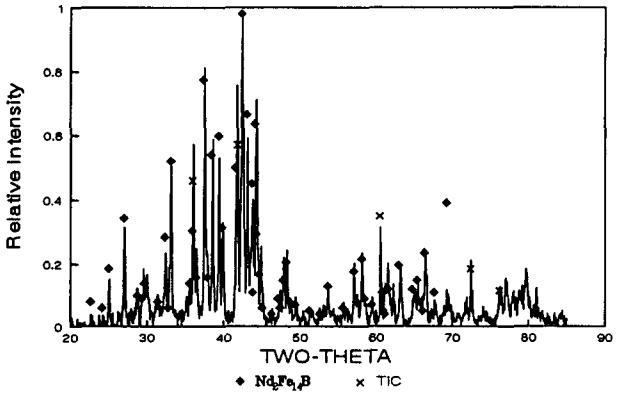

Fig. 12. XRD pattern of the $X = 6$ TiC alloy which has been homogenized at 1000°C for one week.

fine precipitates found throughout the microstructure and the interaction volume of the beam. Nevertheless, this indicates that the equilibrium solubility of Ti with C in the 2–14–1 phase is extremely small.

3.2.3. Stability

By comparing the appearance and size of the TiB_2 and TiC precipitates in the as-cast and homogenized alloys it is apparent that the Ti carbides and borides did not dissolve at high temperatures and that they resist coarsening (Ostwald ripening) up to 1000°C. Both precipitates are candidates for the inhibition or prevention of grain growth. However, TiC seems to form the best dispersion of precipitates since it forms at the grain boundaries as discrete particles while the secondary Ti borides tend to form in a clumped-up fashion as colonies.

4. Summary

In the Nd–Fe–B–Ti system, TiB_2 is the most stable second phase and in the Nd–Fe–B–Ti–C system, TiC is found to be the most stable second phase. While any second phase located at the grain boundaries can provide pinning, alloying with Ti and C seems to be a much better choice compared with alloying with Ti alone. First, the titanium carbides form as discrete particles while the titanium borides form in colonies of precipitates. In addition, Ti with C has extremely low solid solubility which means that after an appropriate heat treatment, TiC precipitates form out of supersaturated solid solution leaving the 2–14–1 phase unalloyed and returning the excellent intrinsic magnetic properties of the 2–14–1 phase. The effects of TiC addition to the 2–14–1 system on the hard magnetic properties has been studied elsewhere [8]. Furthermore Ti with C addition does not alter the base-alloy composition and they can be used to modify existing alloys without changing the properties of the base alloy. When titanium is added alone it will ultimately form TiB_2, which changes the base-alloy composition and additional boron must be added in order to compensate for the loss.

Acknowledgments

The authors would like to express their thanks and gratitude to K.W. Dennis and M.J. Kramer for their technical assistance and guidance. Ames Laboratory is operated for the US Department of Energy by Iowa State University under contract No. W-7405-ENG-821. This investigation was supported by the Director for Energy Research, Office of Basic Sciences.

References

[1] R. Ramesh, G. Thomas and B.M. Ma, *J. Appl. Phys., 64* (1988) 6416–6422.

[2] Tang Weizhong, Zhou Shouzeng and Hu Bing, *J. Magn. Magn. Mater., 94* (1991) 67–73.

[3] A. Manaf, M. Leonowicz, H.A. Davies and R.A. Buckley, *J. Appl. Phys., 70* (1991) 6366–6368.

[4] T. Gladman, *J. Organometallic Chem.*, (1992) 21–24.

[5] Masato Sagawa, Satoshi Hirosawa, Hitoshi Yamamoto, Setsuo Fujimura and Yutaka Matsuura, *Jpn. J. Appl. Phys., 26* (1987) 785–800.

[6] Y. Kitano, J. Shomomura and M. Shimotomai, *J. Appl. Phys., 69* (1991) 6055–6057.

[7] C.J. Yang and R. Ray, *J. Appl. Phys., 63* (1988) 3525–3527.

[8] D.J. Branagan and R.W. McCallum, *J. Magn. Magn. Mater.*, in press.

[9] Karl A. Gschneidner, Jr., and LeRoy Eyring, *Handbook on the Physics and Chemistry of Rare Earths*, Vol. 15, Elsevier, New York, 1991.

[10] David R. Lide, Jr., *Janaf Thermochemical Tables*, 3rd edn., American Chemical Society and the American Institute of Physics, Vol. 14, 1985.

[11] David R. Lide, *Handbook of Chemistry and Physics*, 71st edn., CRC Press, Ann Arbor, MI, 1990–1991.